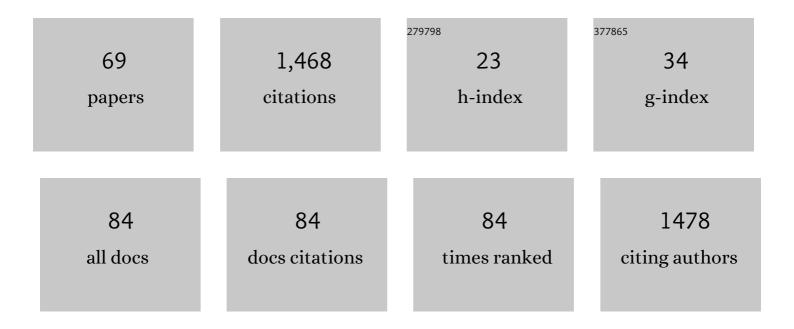
List of Publications by Year in descending order

Source: https://exaly.com/author-pdf/4088729/publications.pdf Version: 2024-02-01



ILANI LINI

#	Article	IF	CITATIONS
1	A New Concept of Radiation Detection Based on a Fluorochromic and Piezochromic Nanocluster. Journal of the American Chemical Society, 2022, 144, 3449-3457.	13.7	29
2	Unveiling the new function of uranyl molecular clusters as fluorometric sensors for UV and X-ray dosimetry. Dalton Transactions, 2022, 51, 3041-3045.	3.3	2
3	Recent advances in the applications of thorium-based metal–organic frameworks and molecular clusters. Dalton Transactions, 2022, 51, 7376-7389.	3.3	19
4	Luminometric dosimetry of X-ray radiation by a zwitterionic uranium coordination polymer. RSC Advances, 2022, 12, 12878-12881.	3.6	1
5	Hydrolytically Stable Zr-Based Metal–Organic Framework as a Highly Sensitive and Selective Luminescent Sensor of Radionuclides. Inorganic Chemistry, 2022, 61, 7467-7476.	4.0	15
6	Tuning of the Network Dimensionality and Photoluminescent Properties in Homo- and Heteroleptic Lanthanide Coordination Polymers. Inorganic Chemistry, 2021, 60, 1359-1366.	4.0	13
7	Boosting the Iodine Adsorption and Radioresistance of Thâ€UiOâ€66 MOFs via Aromatic Substitution. Chemistry - A European Journal, 2021, 27, 1286-1291.	3.3	65
8	Achieving UV and X-ray Dual Photochromism in a Metal–Organic Hybrid via Structural Modulation. ACS Applied Materials & Interfaces, 2021, 13, 2745-2752.	8.0	24
9	Achieving colour tuneable and white-light luminescence in a large family of dual-emission lanthanide coordination polymers. Dalton Transactions, 2021, 50, 14325-14331.	3.3	3
10	Emergence of a thorium–organic framework as a radiation attenuator for selective X-ray dosimetry. Chemical Communications, 2021, 57, 8131-8134.	4.1	12
11	Interpenetration Control in Thorium Metal–Organic Frameworks: Structural Complexity toward Iodine Adsorption. Inorganic Chemistry, 2021, 60, 5617-5626.	4.0	17
12	Visible colorimetric dosimetry of UV and ionizing radiations by a dual-module photochromic nanocluster. Nature Communications, 2021, 12, 2798.	12.8	55
13	Efficiently immobilizing uranium (VI) by oxidized carbon foam. Environmental Science and Pollution Research, 2021, 28, 50471-50479.	5.3	1
14	Thermodynamic non-ideality and disorder heterogeneity in actinide silicate solid solutions. Npj Materials Degradation, 2021, 5, .	5.8	9
15	A cationic thorium–organic framework with triple single-crystal-to-single-crystal transformation peculiarities for ultrasensitive anion recognition. Chemical Science, 2021, 12, 15833-15842.	7.4	20
16	Unveiling the Unique Roles of Metal Coordination and Modulator in the Polymorphism Control of Metalâ€Organic Frameworks. Chemistry - A European Journal, 2021, 27, 17586-17594.	3.3	13
17	Emergence of Thorium-Based Polyoxo Clusters as a Platform for Selective X-ray Dosimetry. Inorganic Chemistry, 2021, 60, 18629-18633.	4.0	8
18	Highly Selective Recovery of Lanthanides by Using a Layered Vanadate with Acid and Radiation Resistance. Angewandte Chemie - International Edition, 2020, 59, 1878-1883.	13.8	31

#	Article	IF	CITATIONS
19	Highly Selective Recovery of Lanthanides by Using a Layered Vanadate with Acid and Radiation Resistance. Angewandte Chemie, 2020, 132, 1894-1899.	2.0	3
20	Unexpected structural complexity of thorium coordination polymers and polyoxo cluster built from simple formate ligands. Inorganic Chemistry Frontiers, 2020, 7, 260-269.	6.0	26
21	Thermodynamic description of the constitutive binaries of the NaCl-KCl-UCl3-PuCl3 system. Calphad: Computer Coupling of Phase Diagrams and Thermochemistry, 2020, 70, 101783.	1.6	22
22	Structural Complexity and Magnetic Orderings in a Large Family of 3d–4f Heterobimetallic Sulfates. Inorganic Chemistry, 2020, 59, 13398-13406.	4.0	6
23	Local structure of uranium in polycrystalline α-U2N3+δ film probed by X-ray absorption spectroscopy. Journal of Nuclear Materials, 2020, 542, 152404.	2.7	1
24	Modulated synthesis and isoreticular expansion of Th-MOFs with record high pore volume and surface area for iodine adsorption. Chemical Communications, 2020, 56, 6715-6718.	4.1	81
25	Unusual Heterometallic Cation-Cation Interactions in Uranyl Zinc Germanates. European Journal of Inorganic Chemistry, 2020, 2020, 2182-2185.	2.0	2
26	Mesoporous Zeolitic Imidazolate Framework-67 Nanocrystals on Siliceous Mesocellular Foams for Capturing Radioactive Iodine. ACS Applied Nano Materials, 2020, 3, 5390-5398.	5.0	33
27	Ultrastable Thorium Metal–Organic Frameworks for Efficient Iodine Adsorption. Inorganic Chemistry, 2020, 59, 4435-4442.	4.0	98
28	Effect of graphite particles in molten LiF-NaF-KF eutectic salt on corrosion behaviour of GH3535 alloy. Corrosion Science, 2020, 168, 108581.	6.6	13
29	Unexpected Roles of Alkali-Metal Cations in the Assembly of Low-Valent Uranium Sulfate Molecular Complexes. Inorganic Chemistry, 2020, 59, 2348-2357.	4.0	11
30	Size-dependent selective crystallization using an inorganic mixed-oxoanion system for lanthanide separation. Dalton Transactions, 2019, 48, 12808-12811.	3.3	16
31	The structural evolution and tunable photoluminescence of f-element bearing coordination polymers of the 2,4,6-tri-1±-pyridyl-1,3,5-triazine ligand. CrystEngComm, 2019, 21, 5059-5066.	2.6	14
32	Polyoxometalates: [Ln ₆ O ₈] Clusterâ€Encapsulating Polyplumbites as New Polyoxometalate Members and Record Inorganic Anionâ€Exchange Materials for ReO ₄ ^{â^²} Sequestration (Adv. Sci. 17/2019). Advanced Science, 2019, 6, 1970105.	11.2	1
33	Investigation of the local structure of molten ThF ₄ –LiF and ThF ₄ –LiF–BeF ₂ mixtures by high-temperature X-ray absorption spectroscopy and molecular-dynamics simulation. Journal of Synchrotron Radiation, 2019, 26, 1733-1741.	2.4	11
34	Corrosion behaviour of 316H stainless steel in molten FLiNaK eutectic salt containing graphite particles. Corrosion Science, 2019, 160, 108174.	6.6	35
35	Expansion of the structural diversity of f-element bearing molybdate iodates: synthesis, structures, and optical properties. Dalton Transactions, 2019, 48, 4823-4829.	3.3	16
36	Insights into the new 3d–5f heterometallic quaternary fluorides: Synthesis, crystal structures, spectroscopic properties, and thermodynamic stability. Inorganica Chimica Acta, 2019, 487, 362-368.	2.4	2

#	Article	IF	CITATIONS
37	[Ln 6 O 8] Clusterâ€Encapsulating Polyplumbites as New Polyoxometalate Members and Record Inorganic Anionâ€Exchange Materials for ReO 4 â^' Sequestration. Advanced Science, 2019, 6, 1900381.	11.2	16
38	Differential interplay between Ce and U on local structures of U1-xCexO2 solid solutions probed by X-ray absorption spectroscopy. Journal of Nuclear Materials, 2019, 515, 238-244.	2.7	6
39	A Large Family of Centrosymmetric and Chiral f-Element-Bearing Iodate Selenates Exhibiting Coordination Number and Dimensional Reductions. Inorganic Chemistry, 2018, 57, 1676-1683.	4.0	23
40	In Situ Reduction from Uranyl Ion into a Tetravalent Uranium Trimer and Hexamer Featuring Ion-Exchange Properties and the Alexandrite Effect. Inorganic Chemistry, 2018, 57, 6753-6761.	4.0	16
41	Uranium-Induced Changes in Crystal-Field and Covalency Effects of Th4+ in Th1–xUxO2 Mixed Oxides Probed by High-Resolution X-ray Absorption Spectroscopy. Inorganic Chemistry, 2018, 57, 11404-11413.	4.0	8
42	Anionic uranyl oxyfluorides as a bifunctional platform for highly selective ion-exchange and photocatalytic degradation of organic dyes. Dalton Transactions, 2018, 47, 14908-14916.	3.3	10
43	Immobilization of Alkali Metal Fluorides via Recrystallization in a Cationic Lamellar Material, [Th(MoO ₄)(H ₂ O) ₄ Cl]Cl·H ₂ O. Inorganic Chemistry, 2018, 57, 6778-6782.	4.0	3
44	A chiral smectic structure assembled from nanosheets and nanorods. Chemical Communications, 2017, 53, 1868-1871.	4.1	27
45	Linking Solution Structures and Energetics: Thorium Nitrate Complexes. Journal of Physical Chemistry B, 2017, 121, 8577-8584.	2.6	9
46	Thorium copper phosphides: more diverse metal–phosphorus and phosphorus–phosphorus interactions than U analogues. Dalton Transactions, 2017, 46, 12041-12052.	3.3	1
47	Influence of Countercation Hydration Enthalpies on the Formation of Molecular Complexes: A Thorium–Nitrate Example. Journal of the American Chemical Society, 2017, 139, 18003-18008.	13.7	33
48	Probing the Influence of Acidity and Temperature to Th(IV) on Hydrolysis, Nucleation, and Structural Topology. Inorganic Chemistry, 2017, 56, 14198-14205.	4.0	12
49	Th ₃ [Th ₆ (OH) ₄ O ₄ (H ₂ O) ₆](SO <su A Self-Assembled Microporous Open-Framework Thorium Sulfate. Inorganic Chemistry, 2016, 55, 10098-10101.</su 	b>4 4.0	•) ₁₂₂₆
50	Why Is Uranyl Formohydroxamate Red?. Inorganic Chemistry, 2015, 54, 5280-5284.	4.0	19
51	Structure–Property Correlations in the Heterobimetallic 4f/3d Materials Ln ₂ M(TeO ₃) ₂ (SO ₄) (Ln = Y, Nd, Sm, Eu, Gd, Tb, Dy, Ho,) Tj E	TQ:m] 10.	7&4314 rg81
52	Graphene-based photocatalysts for oxygen evolution from water. RSC Advances, 2015, 5, 6543-6552.	3.6	23
53	Chirality and Polarity in the fâ€Block Borates M ₄ [B ₁₆ O ₂₆ (OH) ₄ (H ₂ O) ₃ Cl <sub (M=Sm, Eu, Gd, Pu, Am, Cm, and Cf). Chemistry - A European Journal, 2014, 20, 9892-9896.</sub 	>48x.‡sub>]	27
54	Straightforward Reductive Routes to Air-Stable Uranium(III) and Neptunium(III) Materials. Inorganic Chemistry, 2014, 53, 7455-7466.	4.0	12

#	Article	IF	CITATIONS
55	LnV3Te3O15(OH)3·nH2O (Ln = Ce, Pr, Nd, Sm, Eu, Gd; n = 1–2): A New Series of Semiconductors with Mixed-Valent Tellurium (IV,VI) Oxoanions. Inorganic Chemistry, 2014, 53, 9058-9064.	4.0	13
56	Dimensional and Coordination Number Reductions in a Large Family of Lanthanide Tellurite Sulfates. Inorganic Chemistry, 2014, 53, 8555-8564.	4.0	16
57	Ionothermal and Hydrothermal Flux Syntheses of Five New Uranyl Phosphonates. Crystal Growth and Design, 2014, 14, 228-235.	3.0	39
58	Challenges in the Search for Magnetic Coupling in 3d/4f Materials: Syntheses, Structures, and Magnetic Properties of the Lanthanide Copper Heterobimetallic Compounds, RE ₂ Cu(TeO ₃) ₂ (SO ₄) ₂ . Chemistry of Materials, 2014, 26, 2187-2194.	6.7	25
59	Expansion of the Rich Structures and Magnetic Properties of Neptunium Selenites: Soft Ferromagnetism in Np(SeO3)2. Inorganic Chemistry, 2014, 53, 7154-7159.	4.0	12
60	Th(VO ₃) ₂ (SeO ₃) and Ln(VO ₃) ₂ (IO ₃) (Ln = Ce, Pr, Nd, Sm, and Eu): unusual cases of aliovalent substitution. Chemical Communications, 2014, 50, 3668-3670.	4.1	42
61	Fractional iron solubility of aerosol particles enhanced by biomass burning and ship emission in Shanghai, East China. Science of the Total Environment, 2014, 481, 377-391.	8.0	38
62	Synthesis of Divalent Europium Borate via in Situ Reductive Techniques. Inorganic Chemistry, 2013, 52, 8099-8105.	4.0	22
63	Comparisons of Plutonium, Thorium, and Cerium Tellurite Sulfates. Inorganic Chemistry, 2013, 52, 4277-4281.	4.0	39
64	Synthesis, Structure, and Spectroscopy of Two Ternary Uranium(IV) Thiophosphates: UP ₂ S ₉ and UP ₂ S ₇ Containing P ₂ S ₉ ^{2â€"} and P ₂ S ₇ ^{2â€"} Ligands. Inorganic Chemistry, 2013, 52, 7747-7751.	4.0	11
65	Thermochromism, the Alexandrite Effect, and Dynamic Jahn–Teller Distortions in Ho ₂ Cu(TeO ₃) ₂ (SO ₄) ₂ . Inorganic Chemistry, 2013, 52, 13278-13281.	4.0	20
66	Incorporation of Neptunium(VI) into a Uranyl Selenite. Inorganic Chemistry, 2012, 51, 10480-10482.	4.0	13
67	Cerium(IV) Tellurite Halides [Ce ₂ Te ₇ O ₁₇]X ₂ (X =) Tj ETQq1 T Chemistry, 2012, 51, 10083-10085.	0.784314 4.0	4 rgBT /Over 30
68	Unusual Coordination for Plutonium(IV), Cerium(IV), and Zirconium(IV) in the Cationic Layered Materials [M2Te4O11]X2 (M = Pu, Ce, Zr; X = Cl, Br). Inorganic Chemistry, 2012, 51, 11949-11954.	4.0	27
69	Pseudomonas syringae Type III Effector HopZ1 Targets a Host Enzyme to Suppress Isoflavone Biosynthesis and Promote Infection in Soybean. Cell Host and Microbe, 2011, 9, 177-186.	11.0	99